



HAL
open science

Divergent roles of IREG/Ferroportin transporters from the nickel hyperaccumulator *Leucocroton havanensis*

Dubiel Alfonso Gonzalez, Vanesa Sanchez Garcia de la Torre, Rolando Reyes Fernandez, Louise Barreau, Sylvain Merlot

► To cite this version:

Dubiel Alfonso Gonzalez, Vanesa Sanchez Garcia de la Torre, Rolando Reyes Fernandez, Louise Barreau, Sylvain Merlot. Divergent roles of IREG/Ferroportin transporters from the nickel hyperaccumulator *Leucocroton havanensis*. 2023. hal-04274029v1

HAL Id: hal-04274029

<https://hal.science/hal-04274029v1>

Preprint submitted on 7 Nov 2023 (v1), last revised 20 Sep 2024 (v2)

HAL is a multi-disciplinary open access archive for the deposit and dissemination of scientific research documents, whether they are published or not. The documents may come from teaching and research institutions in France or abroad, or from public or private research centers.

L'archive ouverte pluridisciplinaire **HAL**, est destinée au dépôt et à la diffusion de documents scientifiques de niveau recherche, publiés ou non, émanant des établissements d'enseignement et de recherche français ou étrangers, des laboratoires publics ou privés.

Divergent roles of IREG/Ferroportin transporters from the nickel hyperaccumulator

Leucocroton havanensis

Dubiel Alfonso Gonzalez^{1,2*}, Vanesa Sanchez Garcia de la Torre³, Rolando Reyes Fernandez²,
Louise Barreau³, Sylvain Merlot^{3,4*}

¹ *Jardín Botánico Nacional, Universidad de La Habana, Carretera “El Rocío” km 3.5, Calabazar, Boyeros, La Habana, Cuba.*

² *Universidad Agraria de La Habana, Facultad de Agronomía, Autopista Nacional Km 23 ½, 32700, San José de las Lajas, Mayabeque, Cuba.*

³ *Université Paris-Saclay, CEA, CNRS, Institute for Integrative Biology of the Cell (I2BC), 91198, Gif-sur-Yvette, France.*

⁴ *Laboratoire de Recherche en Sciences Végétales (LRSV), UMR5546 CNRS/UPS/INPT, 31320, Auzeville- Tolosane, France.*

* For correspondence: dubiel.alfonso@gmail.com; sylvain.merlot@univ-tlse3.fr

1 **Highlight**

2 The nickel hyperaccumulator *Leucocroton havanensis* endemic to Cuba, expresses two
3 paralogous metal transporters of the IREG/ferroportin family that play distinct but
4 complementary roles in nickel tolerance and accumulation.

5

6 **Abstract**

7

8 In response to our ever-increasing demand for metals, phytotechnologies are being developed
9 to limit the environmental impact of conventional metal mining. However, the development of
10 these technologies, which rely on plant species able to tolerate and accumulate metals, is partly
11 limited by our lack of knowledge of the underlying molecular mechanisms.

12 In this work, we aimed to identify genes involved in nickel hyperaccumulation in the
13 Euphorbiaceae species *Leucocroton havanensis*. Using transcriptomic data, we identified two
14 homologous genes, *LhavIREG1* and *LhavIREG2*, encoding divalent metal transporters of the
15 IREG/ferroportin family. Both genes are expressed at similar levels in shoots, but *LhavIREG1*
16 shows higher expression in roots. Heterologous expression of these transporters in *A. thaliana*
17 revealed that *LhavIREG1* is localized to the plasma membrane, whereas *LhavIREG2* is located
18 at the vacuole. In addition, expression of each gene induced a significant increase in nickel
19 tolerance. Taken together, our data suggest that *LhavIREG2* is involved in nickel sequestration
20 in vacuoles of leaf cells, whereas *LhavIREG1* is mainly involved in nickel translocation from
21 roots to shoots, but could also be involved in metal sequestration in cell walls. Our results
22 suggest that paralogous IREG/ferroportin transporters may play complementary roles in nickel
23 hyperaccumulation in plants.

24

25 **Introduction**

26 Since the beginning of the industrial revolution, and today accelerated by the energy transition
27 required to reduce CO₂ emissions, metal use intensity is increasing exponentially for strategic
28 metals. Metal mining and refining are responsible for the dispersion of metals from primary
29 sites, increasing the risk of contamination in the natural environment and agricultural soils
30 (Dudka and Adriano, 1997; Li *et al.*, 2014; Sonter *et al.*, 2020; Vidal *et al.*, 2022).
31 Phytotechnologies based on plants capable of hyperaccumulating metals have been proposed
32 as a solution to limit the environmental impact of metal mining, remediate contaminated soils
33 and recycle valuable metals (Suman *et al.*, 2018; DalCorso *et al.*, 2019; Corzo Remigio *et al.*,
34 2020). The development of these phytotechnologies is particularly relevant in Mediterranean
35 and tropical regions where nickel mining can have a significant impact on rich biodiversity (van
36 der Ent *et al.*, 2015). As for other crops, a better understanding of the molecular mechanisms
37 involved in metal tolerance and accumulation will support the development of sustainable
38 phytotechnologies using hyperaccumulators.

39 Metal hyperaccumulators are plant species that are able to tolerate and accumulate enormous
40 amounts of metal in their leaves (van der Ent *et al.*, 2013). More than 700 hyperaccumulators
41 have been identified, accumulating a wide variety of metals such as nickel, zinc or manganese.
42 However, nickel hyperaccumulators represent the vast majority of these species (Reeves *et al.*,
43 2018). At the molecular level, metal hyperaccumulation requires high activity of genes involved
44 in metal chelation and transport, from metal uptake by roots to metal storage in leaves (Manara
45 *et al.*, 2020). Accordingly, molecular studies, mostly performed in hyperaccumulators from the
46 Brassicaceae family, suggest that metal hyperaccumulation has evolved from the high and
47 constitutive expression of genes involved in the regulation of metal homeostasis in plants
48 (Becher *et al.*, 2004; Weber *et al.*, 2004; Hammond *et al.*, 2006; Halimaa *et al.*, 2014). For

49 example, zinc hyperaccumulation in *Arabidopsis halleri* has evolved from the triplication of
50 the *heavy metal Atpase 4 (AhHMA4)* gene and mutations in cis-elements leading to high
51 expression of this metal pump. The high activity of *AhHMA4* promotes zinc loading in the
52 xylem and thus efficient translocation of zinc to the shoots (Hanikenne *et al.*, 2008).
53 Interestingly, similar genetic mechanisms are proposed to be at the origin of zinc
54 hyperaccumulation in *Noccaea caerulescens*, suggesting that the high expression of *HMA4* is
55 a convergent mechanism involved in zinc hyperaccumulation in Brassicaceae (Ó Lochlainn *et*
56 *al.*, 2011; Craciun *et al.*, 2012). Recent studies have shown that the high expression of divalent
57 metal ion transporters of the IREG/ferroportin family (IREG/FPN) is repeatedly associated with
58 nickel hyperaccumulation in several plant families (Merlot *et al.*, 2014; Halimaa *et al.*, 2014;
59 Meier *et al.*, 2018; García de la Torre *et al.*, 2021).

60 Plant genomes contain two distinct groups of IREG/FPN transporters (Schaaf *et al.*, 2006;
61 Taniguchi *et al.*, 2015; García de la Torre *et al.*, 2021). The first group, represented by
62 *Arabidopsis thaliana* AtIREG3/MAR1, encodes plastid transporters that are likely involved in
63 the regulation of iron homeostasis in chloroplasts and mitochondria (Conte *et al.*, 2009; Kim *et*
64 *al.*, 2021). The second group, represented by AtIREG1/FPN1 and AtIREG2/FPN2 in *A.*
65 *thaliana*, encodes vacuolar and plasma membrane transporters (Morrissey *et al.*, 2009).
66 AtIREG2/FPN2 was shown to be expressed in roots in response to iron starvation and localized
67 to the vacuolar membrane. The *A. thaliana ireg2* mutant is more sensitive to nickel, suggesting
68 that AtIREG2 transports nickel into vacuoles to limit metal toxicity. Accordingly, plants
69 overexpressing *AtIREG2* are more resistant to nickel and accumulate more of this metal (Schaaf
70 *et al.*, 2006). In contrast, AtIREG1/FPN1 localizes to the plasma membrane and has been
71 proposed to mediate the loading of cobalt into the xylem for long-distance transport to the shoot
72 (Morrissey *et al.*, 2009). However, the *ireg1* mutation further increases the nickel sensitivity
73 associated with *ireg2*, suggesting that AtIREG1 is also capable of transporting nickel. Analysis

74 of orthologous transporters from *Medicago truncatula* (MtFPN2) and from *rice* (OsFPN1)
75 revealed that group 2 IREG/FPN transporters can also be found in endomembranes and Golgi
76 respectively (Escudero *et al.*, 2020; Kan *et al.*, 2022).

77 To date, functional analyses of cellular IREG/FPN transporters associated with nickel
78 hyperaccumulation have suggested that these transporters are involved in the storage of nickel
79 in the vacuole of leaf cells (Merlot *et al.*, 2014; García de la Torre *et al.*, 2021). However, the
80 genomes of several nickel hyperaccumulators contain more than one gene encoding for group
81 2 IREG/FPN transporters. Interestingly, the nickel hyperaccumulator *Leucocroton havanensis*,
82 endemic to Cuba, expresses two genes coding for group 2 IREG/FPN transporters in leaves,
83 whereas the related nonaccumulator species *Leucocroton havanensis* apparently expresses only
84 one gene (Jestrow *et al.*, 2012; García de la Torre *et al.*, 2021). This observation raises the
85 question of the role of homologous group 2 IREG/FPN transporters in nickel
86 hyperaccumulation.

87 In this work, we have studied the function of the two group 2 IREG/FPN transporters,
88 LhavIREG1 and LhavIREG2, identified in the nickel hyperaccumulator *Leucocroton*
89 *havanensis*. Our results indicate that the two genes have distinct expression patterns in roots
90 and shoots and localize to different cellular membranes. Heterologous expression in *A. thaliana*
91 further suggestss that the two genes have different functions in nickel transport and may
92 therefore play distinct but complementary roles in nickel tolerance and accumulation.

93

94

95 **Materials and Methods**

96 *Leucocroton havanensis* plant material

97 *Leucocroton havanensis* seeds were collected from a single female specimen (23°04'55.5"N
98 82°06'46.1"W) growing on ultramafic soil in the ecological reserve “La Coca” (Havana, Cuba).
99 Seeds and young plantlets were grown *in vitro* on Murashige and Skoog agar medium
100 supplemented or not with 3.2 mM NiSO₄ for 6 weeks after germination as previously described
101 (González and Matrella, 2013). Root and shoot samples were collected separately and washed
102 with distilled water. After rapidly removing water with a paper towel, samples were cut into 3
103 mm pieces and immediately placed in RNAlater (Sigma-Aldrich). Samples were transported
104 from Cuba to France and stored at -80°C until processing.

105

106 *Transcriptomic analyses*

107 RNA from *L. havanensis* root and leaf samples treated or not with nickel were extracted using
108 Tri reagent (Sigma-Aldrich). RNA sequencing, *de novo* transcriptome assembly, transcriptome
109 annotation, read mapping and differential gene expression analysis were performed essentially
110 as described previously (García de la Torre *et al.*, 2021). The *de novo* assembly of the
111 transcriptome (Lhav_v2), was performed using RNA-seq reads from root and shoot samples of
112 nickel-treated plantlets. The quality of the assembly was analyzed by the TransRate v1.0.3
113 package using the trimmed read sequences used to assemble Lhav_v2 (Smith-Unna *et al.*,
114 2016). The completeness of the assembled transcriptome was estimated using BUSCO (v 4.0.6)
115 and viridiplantae_odb10 lineage dataset (Seppey *et al.*, 2019). Differential gene expression
116 analysis was performed using the edgeR bioconductor package with TMM normalization and
117 Exact test for statistical analysis, with one repetition per sample. Genes with absolute fold
118 change $|FC| \geq 10$ and adjusted p-value ≤ 0.05 were considered as differentially expressed (DE)
119 genes.

120

121 ***Reconstruction and cloning of LhavIREG coding sequences***

122 The coding sequence of *LhavIREG1* was predicted from transcriptome Lhav_v2 contigs #981
123 and #4486, and from transcriptome Lhav_v1 contigs #820 and #4646. The coding sequence of
124 *LhavIREG2* was predicted from transcriptome Lhav_v2 contig #101 and from transcriptome
125 Lhav_v1 contigs #170 and #14018. The coding sequence of *LhavIREG3* was predicted from
126 transcriptome Lhav_v2 contigs #6824 and #12273, and from transcriptome Lhav_v1 contigs
127 #8277, #9347 and #4646.

128 The coding sequences of *LhavIREG1* and *LhavIREG2* were amplified from leaf cDNA using
129 high-fidelity Phusion polymerase (Thermo Scientific) with gene-specific primers containing
130 the attB recombination sequences attB1_LhavIREG1_For/attB2_LhavIREG1_Rev-(no)stop
131 and attB1_LhavIREG2_For/attB2_LhavIREG2_Rev-(no)stop respectively (Table S1). The
132 PCR products were recombined into pDONOR207 using GATEWAY technology (Invitrogen)
133 to generate pDON207-*LhavIREG1(no)stop* and pDON207-*LhavIREG2(no)stop*. We confirmed
134 the predicted sequences of the *LhavIREG1* and *LhavIREG2* coding regions by double-strand
135 Sanger sequencing (GATC-Eurofins).

136

137 ***Phylogenetic analysis***

138 Sequences for IREG/FPN proteins were obtained from Dicots Plaza 5.0 (Van Bel *et al.*, 2022),
139 for *Arabidopsis thaliana* AthaIREG1 (AT5G03570), AthaIREG2 (AT2G38460), AthaIREG3
140 (AT5G26820); *Arabidopsis lyrata* AlyrIREG1 (AL4G35730), AlyrIREG2 (AL6G13070),
141 AlyrIREG3 (AL6G38700); *Eutrema salsugineum* EsalIREG1 (Thhalv10013299m.g),
142 EsalIREG2 (Thhalv10016525m.g), EsalIREG3 (Thhalv10003867m.g); *Teobroma cacao*
143 TcacIREG1 (Thecc.05G005200), TcacIREG2 (Thecc.05G005300), TcacIREG3
144 (Thecc.05G323900); *Cucumis melo* CmelIREG1 (MELO3C026034.2), CmelIREG3

145 (MELO3C004177.2); *Phaseolus vulgaris* PvulIREG1 (Phvul.010G062200), PvulIREG2
146 (Phvul.010G062300), PvulIREG3 (Phvul.007G201800); *Nicotiana tabacum* NtabIREG1
147 (Nitab4.5_0000355g0170), NtabIREG2 (Nitab4.5_0012987g0010), NtabIREG3_1
148 (Nitab4.5_0001338g0110), NtabIREG3_2 (Nitab4.5_0004525g0030); *Chenopodium quinoa*
149 CquiIREG1 (AUR62006302), CquiIREG2 (AUR62026347), CquiIREG3_1 (AUR62000385),
150 CquiIREG3_2 (AUR62006741) and *Erigeron canadensis* EcanIREG1 (ECA247G0592). The
151 sequences of *Ricinus communis* RcomIREG1 (XP_048225718.1), RcomIREG2
152 (XP_048235846.1), RcomIREG3 (XP_002512519.1) and *Homo sapiens* HsapFPN
153 (XP_047300022.1) were obtained from NCBI. The sequences of *Leucocroton havanensis*
154 LhavIREG1, LhavIREG2 proteins were translated from the corresponding cDNA sequences
155 (OR234317, OR234318). The sequence of LhavIREG3 was deduced from the corresponding
156 contigs. Protein alignment was performed with CLC Genomics Workbench 22.0.1 (Qiagen)
157 using MUSCLE v3.8.425 (Edgar, 2004). The tree was constructed using maximum likelihood
158 phylogeny (neighbor-joining, 100 bootstrap replicates) and displayed using iTol v6 (Letunic
159 and Bork, 2021).

160

161 ***Quantification of gene expression by RT-qPCR***

162 Total RNA was extracted with TRI reagent according to the manufacturer's instructions
163 (Sigma-Aldrich) and purified with RNeasy Plant Mini Kit on-column DNase I treatment
164 (Qiagen). cDNA synthesis, quantitative PCR amplification and analysis were performed as
165 previously described (García de la Torre *et al.*, 2021). The expression of *LhavIREG1* and
166 *LhavIREG2* was normalized to the expression of the *histidine kinase 3* gene (*LhavH3K*;
167 Lhav_v2 contig #1232), which was chosen as a reference because of its stable expression in
168 our transcriptomic data. Primers used for RT-qPCR experiments are given in Table S1. The
169 relative expression of *LhavIREG1* and *LhavIREG2* was quantified according to Pfaffl (2001).

170

171 ***Analysis of LhavIREG1 and LhavIREG2 activity in yeast***

172 pDON207-*LhavIREG1stop* and pDON207-*LhavIREG2stop* were recombined with pDR195-
173 GTW (Oomen *et al.*, 2009) to generate pDR195-*LhavIREG1* and pDR195-*LhIREG2*. These
174 constructs were transformed together with pDR195-GTW and pDR195-*AtIREG2* (Schaaf *et al.*,
175 2006) into *Saccharomyces cerevisiae* strain Y00000H strain (BY4741; *MATa*; *leu2Δ*; *met15Δ*;
176 *ura3Δ*). Nickel accumulation in yeast was essentially determined as previously described
177 (Merlot *et al.*, 2014; García de la Torre *et al.*, 2021). Yeast cells were grown in 50 ml of liquid
178 SD-Ura medium supplemented with 400 μ M NiCl₂ for 30 h at 28 °C with vigorous shaking.
179 Cells were harvested by centrifugation at 4 °C and pellets were washed twice with ice-cold [10
180 mM EDTA, 20 mM MES pH 5.5] and once with ice-cold ultrapure water. Yeast pellets were
181 dried at 65°C prior to elemental analysis.

182

183 ***Expression of LhavIREG1 and LhavIREG2 in Arabidopsis thaliana***

184 pDON207-*LhavIREG1nostop* and pDON207-*LhavIREG2nostop* were recombined with the
185 plant expression vector pMUBI83 (Merlot *et al.*, 2014) to express C-terminal protein fusions
186 with the green fluorescent protein (GFP). Both constructs pMUBI83-*LhavIREG1* and
187 pMUBI83-*LhIREG2* were transformed into the *A. thaliana ireg2-1* mutant (Schaaf *et al.*, 2006)
188 as described previously (Merlot *et al.*, 2014). For each construct, three homozygous, single
189 locus insertion, T3 lines, expressing the fluorescent protein were selected. T3 lines together
190 with *ireg2-1* and WT (Col) were grown *in vitro* for 10 days on Hoagland agar medium
191 containing 10 μ M Fe-HBED and supplemented with 30 or 50 μ M NiCl₂. Primary root length
192 was measured as described previously (Merlot *et al.*, 2014). To measure metal accumulation,
193 plants were grown on Hoagland agar medium containing 10 μ M Fe-HBED for 7 days and then

194 transferred to the same medium supplemented with 50 μ M NiCl₂ for 5 days. Roots and shoots
195 samples were prepared for elemental analyses as previously described (Merlot *et al.*, 2014).

196

197 *Quantitative elemental analyses*

198 The dry weight of yeast and plant samples was measured before mineralization in 2 ml of 70%
199 HNO₃ for 4 h at 120 °C. Samples were diluted with ultrapure water to a total volume of 12 ml,
200 and metal content was measured using a 4200 MP-AES spectrophotometer (Agilent
201 technologies) as previously described (García de la Torre *et al.*, 2021).

202

203 *Confocal imaging*

204 Roots of *ireg2-1* transgenic T₂ lines transformed with pMUBI83-*LhavIREG1* and pMUBI83-
205 *LhavIREG2* were imaged on a Leica SP8X inverted confocal microscope (IMAGERIE-Gif
206 platform www.i2bc.paris-saclay.fr/bioimaging/) as previously described (Merlot *et al.* 2014),
207 with laser excitation at 490 nm and collection of emitted light at 500-550nm for GFP and
208 600-650 nm for propidium iodide.

209

210 *Statistics*

211 GraphPad (v7.05) and the shiny application SuperPlotsOfData (Lord *et al.*, 2020) were used
212 for ttatistical analyses and data presentation.

213

214 **Results**

215 **Analysis of leaf and root transcriptomes of *Leucocroton havanensis***

216 In a previous study, we generated the leaf transcriptome of *Leucocroton havanensis* (Lhav_v1)
217 and compared it with the leaf transcriptome of the related nonaccumulator species *Lasiocroton*
218 *microphyllus* to identify genes associated with the nickel hyperaccumulation trait (García de la
219 Torre *et al.*, 2021). In this study, we wanted to deepen our knowledge of the root and shoot
220 mechanisms involved in nickel hyperaccumulation in *L. havanensis*. We sequenced RNA from
221 roots and shoots to generate a new transcriptome assembly for this nickel hyperaccumulator
222 species (Lhav_v2). This assembly consists of 65936 contigs with 14320 contigs larger than 1kb
223 (Table 1). 31936 contigs (48%) were annotated with Blast2GO and 12771 contigs (19%) with
224 Mercator 4. We then used this transcriptome as a reference to analyze the effect of nickel on
225 gene expression in *L. havanensis* (Figure 1, Table S2). We identified 27 contigs differentially
226 expressed (DE) in response to nickel in roots (Figure 1B), indicating a limited effect of nickel
227 hyperaccumulation on gene expression in this tissue. Among the 19 contigs up-regulated in
228 response to nickel in roots, contigs encoding for seed storage proteins (MapMan4 category
229 19.5.1) are overrepresented (4 contigs, FDR adj. p-value = 3.1e-07). In contrast, we identified
230 442 DE contigs in shoots, with 170 contigs up- and 272 contigs down-regulated in response to
231 nickel (Figure 1A). This result suggests that nickel accumulation has a more pronounced effect
232 on the shoot transcriptome. However, we could not identify enriched functional categories
233 among DE contigs in shoots. In particular, we did not identify any DE contigs encoding proteins
234 involved in metal homeostasis.

235

236 ***IREG/ferroportin genes in Leucocroton havanensis***

237 IREG/FPN transporters have previously been implicated in nickel tolerance and accumulation
238 in plants (Schaaf *et al.*, 2006; Merlot *et al.*, 2014; Meier *et al.*, 2018; García de la Torre *et al.*,

239 2021). Using *Leucocroton havanensis* transcriptome assemblies, we reconstructed the sequence
240 of IREG/FPN genes expressed in this species. We identified 2 distinct transcripts coding for
241 IREG/ferroportin transporters orthologous to *A. thaliana* AtIREG1 and AtIREG2. These
242 transporters, subsequently named LhavIREG1 and LhavIREG2, belong to the Plaza
243 orthologous group (OG) ORTHO05D005013, which corresponds to group 2 IREG/FPN
244 (Figure 2; Figure S1). We identified a third transporter, LhavIREG3, orthologous to the
245 plastidic (group 1) AtIREG3 transporter and belonging to OG ORTHO05D008050. Analysis
246 of the phylogenetic tree obtained with plant IREG/FPN indicates that LhavIREG1 and
247 LhavIREG2 originated from a duplication of an IREG/FPN ancestral gene in the
248 Euphorbiaceae, independent of the duplication that occurred in the Brassicaceae and gave rise
249 to the paralogous groups represented by AtIREG1 and AtIREG2. It is therefore not possible to
250 infer the function of the *Leucocroton havanensis* IREG/FPN transporters from the known
251 function of AtIREG1 and AtIREG2, which act at the plasma membrane and vacuole
252 respectively (Schaaf *et al.*, 2006; Morrissey *et al.*, 2009).

253

254 ***Analysis of LhavIREG1 and LhavIREG2 expression in Leucocroton havanensis***

255 We analyzed the expression of *LhavIREG1* and *LhavIREG2* in *L. havanensis* by RT-qPCR
256 (Figure 3). This analysis revealed that both genes are expressed at a similar level in shoots but
257 that *LhavIREG1* is more expressed than *LhavIREG2* in roots. These results are supported by
258 the analysis of RNA-Seq data (Table S2). Based on RNA-Seq data, we did not observe a
259 significant effect of nickel on the expression of IREG/FPN genes in *L. havanensis* (Figure 1).
260 These results suggest that both genes are constitutively expressed in *L. havanensis* and that
261 *LhavIREG1* predominantly acts in roots while both genes are likely playing a function in leaves.

262

263 ***LhavIREG1 and LhavIREG2 act as nickel exporters***

264 We have previously shown that *LhavIREG2* expression in yeast increases nickel tolerance
265 (García de la Torre *et al.*, 2021). To further characterize the activity of LhavIREG2 and
266 LhavIREG1, we measure nickel accumulation in yeast cells expressing each of these
267 transporters (Figure 4). The expression of both LhavIREG1 and LhavIREG2 reduces nickel
268 accumulation compared to yeast transformed with the control vector. The same result is
269 observed with *A. thaliana* AtIREG2. These results suggest that both LhavIREG1 and
270 LhavIREG2 transport nickel out of yeast cells, which is consistent with the conserved role of
271 IREG/FPN as divalent metal exporters.

272

273 ***LhavIREG1 and LhavIREG2 localize to different membranes in plant cells***

274 To analyze the localization of LhavIREG1 and LhavIREG2 in plant cells, we fused the two
275 transporters with the green fluorescent protein (GFP) at the C-terminal end and expressed the
276 fusion proteins in the *A. thaliana ireg2* mutant. Root cells of the transgenic T2 lines were
277 imaged by confocal microscopy (Figure 5). Lines expressing LhavIREG1-GFP show a thin
278 GFP fluorescent signal delineating the periphery of the root cells (Figure 5 A, B). This signal
279 indicates that LhavIREG1 is mainly localized to the plasma membrane. In contrast, the GFP
280 signal associated with the expression of LhavIREG2-GFP outlines large cytoplasmic vesicles,
281 suggesting a vacuolar localization (Figure 5 C, D). These results indicate that LhavIREG1 and
282 LhavIREG2 localize to different membranes and therefore likely have distinct cellular
283 functions.

284

285 ***Expression of LhavIREG1 and LhavIREG2 in A. thaliana differentially affects nickel***
286 ***sensitivity and accumulation***

287 We used the same *ireg2* transgenic lines expressing *LhavIREG1-GFP* and *LhavIREG2-GFP* to
288 study the effect of the ubiquitous expression of these transporters on nickel tolerance and
289 accumulation (Figure 6). As observed in previous works (Schaaf *et al.*, 2006; Merlot *et al.*,
290 2014), the *A. thaliana ireg2* mutant is more sensitive to root growth in the presence of nickel
291 than the wild type (Figure 6A, B, C). Expression of both *LhavIREG1-GFP* and *LhavIREG2-*
292 *GFP* in *ireg2* significantly increases root growth in the presence of 30 μ M nickel compared to
293 *ireg2* or the wild-type (Figure 6A, B, C, D). In addition, transgenic lines expressing
294 *LhavIREG1-GFP* and *LhavIREG2-GFP* do not exhibit the chlorotic phenotype observed in
295 *ireg2* leaves in the presence of nickel. Transgenic lines expressing *LhavIREG1-GFP* show a
296 strong tolerance to 50 μ M nickel, a concentration that strongly affects the root growth of the
297 other genotypes (Figure 6D).

298 To further characterize these transgenic lines, we measured nickel accumulation in both roots
299 and shoots (Figure 6E, F). The *ireg2* mutant, which is impaired in the vacuolar sequestration of
300 nickel in roots, translocates and accumulates more nickel in shoots (Schaaf *et al.*, 2006; Merlot
301 *et al.*, 2014). Expression of the vacuolar *LhavIREG2* in *ireg2* transgenic lines slightly increases
302 nickel accumulation in roots, but does not restore nickel accumulation as in wild type ($p=0.02$),
303 indicating a partial complementation of the *ireg2* phenotype. In contrast, expression of
304 *LhavIREG1* further reduces nickel accumulation in roots compared to the *ireg2* mutant
305 ($p=0.03$). In these experiments, we cannot observe a significant effect of *LhavIREG1-GFP* and
306 *LhavIREG2-GFP* expression on nickel accumulation in leaves compared to *ireg2* (Figure 6F),
307 but plants expressing *LhavIREG1-GFP* accumulate significantly more nickel in leaves than
308 wild type ($p=0.02$). These results indicate that the ubiquitous expression of both *LhavIREG1*
309 and *LhavIREG2* leads to a large increase in nickel tolerance, albeit through different cellular
310 mechanisms.

311

312 Discussion

313 In this work, we provided new molecular insights into the mechanisms involved in nickel
314 hyperaccumulation in the Cuban endemic species *Leucocroton havanensis* (Jestrow *et al.*,
315 2012; González and Matrella, 2013). We generated a novel transcriptome assembly containing
316 genes expressed in roots and shoots in this species (Table 1). Using this assembly as a reference,
317 we examined the expression of genes in response to nickel treatment and thus nickel
318 hyperaccumulation (Fig. 1). Our results indicate that nickel treatment elicits a more complex
319 response in shoots (442 DE genes) than in roots (27 DE genes). Enrichment analysis revealed
320 that genes encoding for seed storage proteins are induced by nickel in roots. The biological
321 significance of this response is unclear. No other functional category, including the regulation
322 of metal homeostasis, is enriched in response to nickel. In recent years, metal transporters of
323 the IREG/FPN family have been identified as candidate genes involved in nickel tolerance and
324 accumulation (Schaaf *et al.*, 2006; Merlot *et al.*, 2014; Meier *et al.*, 2018; García de la Torre *et*
325 *al.*, 2021). Analysis of the expression of the two genes encoding group 2 IREG/FPN
326 transporters, *LhavIREG1* and *LhavIREG2*, indicates that both genes are significantly expressed
327 in *L. havanensis*, but are not regulated at the transcriptional level by nickel (Fig. 1, 3). These
328 results are in line with a model suggesting that nickel hyperaccumulation at the species level is
329 associated with a high and constitutive expression of genes involved in metal homeostasis and
330 transport (Verbruggen *et al.*, 2009; Krämer, 2010).

331 We further investigated the putative function of *LhavIREG1* and *LhavIREG2* in nickel
332 hyperaccumulation. Our data showed that *LhavIREG1* and *LhavIREG2* are both nickel
333 exporters (Fig. 4), but localize to the plasma membrane and the vacuole, respectively (Fig. 5).
334 The equivalent dual localization was previously observed for *Arabidopsis thaliana* *AthaIREG1*
335 and *AthaIREG2* (Schaaf *et al.*, 2006; Morrissey *et al.*, 2009). This observation suggests that in
336 these two distant genera, the duplication of an ancestral group 2 IREG/FPN gene resulted in

337 two transporters that convergently evolved into a plasma membrane and a vacuolar form. The
338 molecular determinants of the localization of the IREG/FPN transporters are not yet known.
339 Recently, the presence of a dileucine motif [D/E]X₃₋₅L[L/I] (Bonifacino and Traub, 2003;
340 Komarova *et al.*, 2012) was shown to be involved in the vacuolar localization of *A. thaliana*
341 NRAMP3 and NRAMP4 transporters (Müdsam *et al.*, 2018). At least three canonical dileucine
342 motifs are found in the large cytoplasmic loop and C-terminal extension of LhavIREG2 but not
343 LhavIREG1 (Fig. S1). Further studies will be required to support the role of these motifs in the
344 vacuolar localization of LhavIREG2.

345 As anticipated, ectopic and constitutive expression of the vacuolar LhavIREG2 increases nickel
346 tolerance in the *A. thaliana ireg2* mutant. Surprisingly, expression of the plasma membrane
347 LhavIREG1 increases nickel tolerance to a greater extent (Fig. 6). Elemental analysis indicates
348 that LhavIREG1 expression further reduces nickel accumulation in roots compared to *ireg2* and
349 simultaneously increases accumulation in shoots. These results suggest that ectopic expression
350 of LhavIREG1 does not drive the export of nickel from root cells, but rather promotes its
351 translocation to the shoots. This proposed function of LhavIREG1 in metal translocation was
352 previously proposed for *A. thaliana* IREG1 (Morrissey *et al.*, 2009). *A. thaliana ireg2* plants
353 expressing LhavIREG1 show no symptoms of nickel toxicity in leaves, suggesting nickel is
354 accumulated in a compartment where it is less toxic. Since LhavIREG1 localizes to the plasma
355 membrane, we propose that nickel is exported out of leaf cells and bound to the cell wall.
356 Further experiments, including elemental imaging, would be required to support this
357 hypothesis. Interestingly, while vacuolar sequestration of nickel is recognized as an essential
358 function for nickel tolerance and hyperaccumulation (Schaaf *et al.*, 2006; Merlot *et al.*, 2014;
359 García de la Torre *et al.*, 2021), nickel is also associated with the cell wall in leaves of several
360 hyperaccumulators (Krämer *et al.*, 2000; Bidwell *et al.*, 2004; van der Ent *et al.*, 2019). Taken
361 together, our data suggest that in addition to vacuolar IREG/Ferroportin transporters, plasma

362 membrane IREG/FPN also play an important role in hyperaccumulation, mediating efficient
363 translocation of nickel from roots to shoots and nickel export from leaf cells to limit its toxicity.
364

365 **Data and code availability**

366 The data discussed in this publication have been deposited in NCBI's Gene Expression
367 Omnibus (Edgar *et al.*, 2002) and are accessible through GEO Series accession number
368 GSE237255 (<https://www.ncbi.nlm.nih.gov/geo/query/acc.cgi?acc=GSE237255>). Previous
369 Leucocroton data (Lhav_v1) are available through GEO GSE116049. *LhavIREG1* and
370 *LhavIREG2* cDNA sequences were deposited to GenBank under OR234317 and OR234318
371 accession numbers respectively.

372

373 **Contributions**

374 DAG and SM: conceptualization; DAG, VSGT and SM: methodology; DAG, VSGT and SM:
375 formal analysis; DAG, VSGT, RRF, LB and SM: investigation; DAG: resources; VSGT and
376 SM: data curation; DAG and SM: writing - review & editing; DAG, VSGT and SM:
377 visualization; DAG, VSGT and SM: supervision; SM: funding acquisition.

378

379 **Acknowledgement / Funding**

380 We thank Ludivine Soubigou-Taconnat for the coordination of the *Leucocroton havanensis*
381 RNA sequencing at the POPS platform (Orsay, France), Celeste Belloeil for help with data
382 presentation and Sébastien Thomine for comments on the manuscript. This work was supported
383 by the ANR funding EvoMetoNicks (ANR-13-ADAP-0004) and the MITI-CNRS Defi
384 Enviromics GENE-4-CHEM to S.M. D.A.G and R.R.F were recipient of SCAC mobility
385 fellowships from the French Embassy in Cuba

Bibliography

Becher M, Talke IN, Krall L, Krämer U. 2004. Cross-species microarray transcript profiling reveals high constitutive expression of metal homeostasis genes in shoots of the zinc hyperaccumulator *Arabidopsis halleri*. *Plant J* **37**, 251–268.

Bidwell SD, Crawford SA, Woodrow IE, Sommer-Knudsen J, Marshall AT. 2004. Sub-cellular localization of Ni in the hyperaccumulator, *Hybanthus floribundus* (Lindley) F. Muell. *Plant, Cell and Environment* **27**, 705–716.

Bonifacino JS, Traub LM. 2003. Signals for Sorting of Transmembrane Proteins to Endosomes and Lysosomes. *Annual Review of Biochemistry* **72**, 395–447.

Conte S, Stevenson D, Furner I, Lloyd A. 2009. Multiple antibiotic resistance in *Arabidopsis* is conferred by mutations in a chloroplast-localized transport protein. *Plant physiology* **151**, 559–573.

Corzo Remigio A, Chaney RL, Baker AJM, Edraki M, Erskine PD, Echevarria G, van der Ent A. 2020. Phytoextraction of high value elements and contaminants from mining and mineral wastes: opportunities and limitations. *Plant and Soil* **449**, 11–37.

Craciun AR, Meyer C-L, Chen J, Roosens N, De Groot R, Hilson P, Verbruggen N. 2012. Variation in HMA4 gene copy number and expression among *Noccaea caerulescens* populations presenting different levels of Cd tolerance and accumulation. *Journal of Experimental Botany* **63**, 4179–4189.

DalCorso G, Fasani E, Manara A, Visioli G, Furini A. 2019. Heavy Metal Pollutions: State of the Art and Innovation in Phytoremediation. *International Journal of Molecular Sciences* **20**, 3412.

Dudka S, Adriano DC. 1997. Environmental Impacts of Metal Ore Mining and Processing: A Review. *Journal of Environmental Quality* **26**, 590–602.

Edgar RC. 2004. MUSCLE: multiple sequence alignment with high accuracy and high

throughput. *Nucleic Acids Research* **32**, 1792–1797.

Edgar R, Domrachev M, Lash AE. 2002. Gene Expression Omnibus: NCBI gene expression and hybridization array data repository. *Nucleic Acids Research* **30**, 207–210.

van der Ent A, Baker AJM, Reeves RD, et al. 2015. Agromining: Farming for Metals in the Future? *Environmental Science & Technology* **49**, 4773–4780.

van der Ent A, Baker AJM, Reeves RD, Pollard AJ, Schat H. 2013. Hyperaccumulators of metal and metalloid trace elements: Facts and fiction. *Plant and Soil* **362**, 319–334.

van der Ent A, Spiers KM, Brueckner D, Echevarria G, Aarts MGM, Montargès-Pelletier E. 2019. Spatially-resolved localization and chemical speciation of nickel and zinc in *Noccaea tymphaea* and *Bornmuellera emarginata*. *Metallomics* **11**, 2052–2065.

Escudero V, Abreu I, Tejada-Jiménez M, et al. 2020. *Medicago truncatula* Ferroportin2 mediates iron import into nodule symbiosomes. *New Phytologist* **228**, 194–209.

García de la Torre VS, Majorel-Loulergue C, Rigai G, et al. 2021. Wide cross-species RNA-Seq comparison reveals convergent molecular mechanisms involved in nickel hyperaccumulation across dicotyledons. *New Phytologist* **229**, 994–1006.

González DA, Matrella S. 2013. Nickel hyperaccumulation ‘in vitro’ by *Leucocroton havanensis* (Euphorbiaceae) / Hiperacumulación ‘in vitro’ de Ni en *Leucocroton havanensis* (Euphorbiaceae). *Revista del Jardín Botánico Nacional* **34/35**, 83–88.

Halimaa P, Lin Y-F, Ahonen VH, et al. 2014. Gene expression differences between *Noccaea caerulescens* ecotypes help to identify candidate genes for metal phytoremediation. *Environmental science & technology* **48**, 3344–53.

Hammond JP, Bowen HC, White PJ, Mills V, Pyke KA, Baker AJM, Whiting SN, May ST, Broadley MR. 2006. A comparison of the *Thlaspi caerulescens* and *Thlaspi arvense* shoot transcriptomes. *New Phytologist* **170**, 239–260.

Hanikenne M, Talke IN, Haydon MJ, Lanz C, Nolte A, Motte P, Kroymann J, Weigel D,

Krämer U. 2008. Evolution of metal hyperaccumulation required cis-regulatory changes and triplication of HMA4. *Nature* **453**, 391–395.

Jestrow B, Gutiérrez Amaro J, Francisco-Ortega J. 2012. Islands within islands: a molecular phylogenetic study of the Leucocroton alliance (Euphorbiaceae) across the Caribbean Islands and within the serpentinite archipelago of Cuba. *Journal of Biogeography* **39**, 452–464.

Kan M, Fujiwara T, Kamiya T. 2022. Golgi-Localized OsFPN1 is Involved in Co and Ni Transport and Their Detoxification in Rice. *Rice* **15**, 36.

Kim LJ, Tsuyuki KM, Hu F, et al. 2021. Ferroportin 3 is a dual-targeted mitochondrial/chloroplast iron exporter necessary for iron homeostasis in Arabidopsis. *The Plant Journal* **107**, 215–236.

Komarova NY, Meier S, Meier A, Grottemeyer MS, Rentsch D. 2012. Determinants for Arabidopsis Peptide Transporter Targeting to the Tonoplast or Plasma Membrane. *Traffic* **13**, 1090–1105.

Krämer U. 2010. Metal Hyperaccumulation in Plants. *Annual Review of Plant Biology* **61**, 517–534.

Krämer U, Pickering IJ, Prince RC, Raskin I, Salt DE. 2000. Subcellular Localization and Speciation of Nickel in Hyperaccumulator and Non-Accumulator Thlaspi Species. *Plant Physiology* **122**, 1343–1354.

Letunic I, Bork P. 2021. Interactive Tree Of Life (iTOL) v5: an online tool for phylogenetic tree display and annotation. *Nucleic Acids Research* **49**, W293–W296.

Li Z, Ma Z, van der Kuijp TJ, Yuan Z, Huang L. 2014. A review of soil heavy metal pollution from mines in China: Pollution and health risk assessment. *Science of The Total Environment* **468–469**, 843–853.

Lord SJ, Velle KB, Mullins RD, Fritz-Laylin LK. 2020. SuperPlots: Communicating

reproducibility and variability in cell biology. *Journal of Cell Biology* **219**.

Manara A, Fasani E, Furini A, DalCorso G. 2020. Evolution of the metal

hyperaccumulation and hypertolerance traits. *Plant, Cell & Environment* **43**, 2969–2986.

Meier SK, Adams N, Wolf M, Balkwill K, Muasya AM, Gehring CA, Bishop JM, Ingle

RA. 2018. Comparative RNA-seq analysis of nickel hyperaccumulating and non-accumulating populations of *Senecio coronatus* (Asteraceae). *The Plant Journal* **95**, 1023–1038.

Merlot S, Hannibal L, Martins S, Martinelli L, Amir H, Lebrun M, Thomine S. 2014.

The metal transporter PgIREG1 from the hyperaccumulator *Psychotria gabriellae* is a candidate gene for nickel tolerance and accumulation. *J Exp Bot* **65**, 1551–1564.

Morrissey J, Baxter IR, Lee J, Li L, Lahner B, Grotz N, Kaplan J, Salt DE, Guerinot M

Lou. 2009. The Ferroportin Metal Efflux Proteins Function in Iron and Cobalt Homeostasis in *Arabidopsis*. *The Plant Cell* **21**, 3326–3338.

Müdsam C, Wollschläger P, Sauer N, Schneider S. 2018. Sorting of *Arabidopsis* NRAMP3

and NRAMP4 depends on adaptor protein complex AP4 and a dileucine-based motif. *Traffic* **19**, 503–521.

Ó Lochlainn S, Bowen HC, Fray RG, Hammond JP, King GJ, White PJ, Graham NS,

Broadley MR. 2011. Tandem Quadruplication of HMA4 in the Zinc (Zn) and Cadmium (Cd)

Hyperaccumulator *Noccaea caerulescens* (I Baxter, Ed.). *PLoS ONE* **6**, e17814.

Oomen RJFJ, Wu J, Lelièvre F, Blanchet S, Richaud P, Barbier-Brygoo H, Aarts

MGM, Thomine S. 2009. Functional characterization of NRAMP3 and NRAMP4 from the metal hyperaccumulator *Thlaspi caerulescens*. *New Phytologist* **181**, 637–650.

Pfaffl MW. 2001. A new mathematical model for relative quantification in real-time RT-PCR. *Nucleic Acid Research* **29**, 16–21.

Reeves RD, Baker AJM, Jaffré T, Erskine PD, Echevarria G, Ent A. 2018. A global

database for plants that hyperaccumulate metal and metalloid trace elements. *New Phytologist* **218**, 407–411.

Schaaf G, Honsbein A, Meda AR, Kirchner S, Wipf D, von Wirén N. 2006. AtIREG2 Encodes a Tonoplast Transport Protein Involved in Iron-dependent Nickel Detoxification in *Arabidopsis thaliana* Roots. *Journal of Biological Chemistry* **281**, 25532–25540.

Seppely M, Manni M, Zdobnov EM. 2019. BUSCO: Assessing Genome Assembly and Annotation Completeness BT - Gene Prediction: Methods and Protocols. In: Kollmar M, ed. New York, NY: Springer New York, 227–245.

Smith-Unna R, Bournnell C, Patro R, Hibberd J, Kelly S. 2016. TransRate: reference free quality assessment of de novo transcriptome assemblies. *Genome Research* **26**, 1134–1144.

Sonter LJ, Dade MC, Watson JEM, Valenta RK. 2020. Renewable energy production will exacerbate mining threats to biodiversity. *Nature Communications* **11**, 6–11.

Suman J, Uhlik O, Viktorova J, Macek T. 2018. Phytoextraction of Heavy Metals: A Promising Tool for Clean-Up of Polluted Environment? *Frontiers in Plant Science* **9**, 1–15.

Taniguchi R, Kato HE, Font J, Deshpande CN, Wada M, Ito K, Ishitani R, Jormakka M, Nureki O. 2015. Outward- and inward-facing structures of a putative bacterial transition-metal transporter with homology to ferroportin. *Nature Communications* **6**, 1–10.

Verbruggen N, Hermans C, Schat H. 2009. Molecular mechanisms of metal hyperaccumulation in plants. *New Phytol* **181**, 759–776.

Vidal O, Le Boulzec H, Andrieu B, Verzier F. 2022. Modelling the demand and access of mineral resources in a changing world. *Sustainability (Switzerland)* **14**, 1–16.

Weber M, Harada E, Vess C, Roepenack-Lahaye E V, Clemens S. 2004. Comparative microarray analysis of *Arabidopsis thaliana* and *Arabidopsis halleri* roots identifies nicotianamine synthase, a ZIP transporter and other genes as potential metal hyperaccumulation factors. *The Plant Journal* **37**, 269–281.

Table 1 : Parameters of *Leucocroton havanensis* transcriptome assembly (Lhav_v2)

Contig metrics	
Number of contigs	65936
Number over 1kb	14320
Mean length (kb)	757
N50 (kb)	1196
Read mapping metrics	
Fragment mapped (%)	87
Good mapping (%)	76
Transrate score	
	0.34
Good contigs (%)	95
Busco score (%)	
	69.6
S: 68.7%, D: 0.9%, F: 25.2%, M: 6.1%	

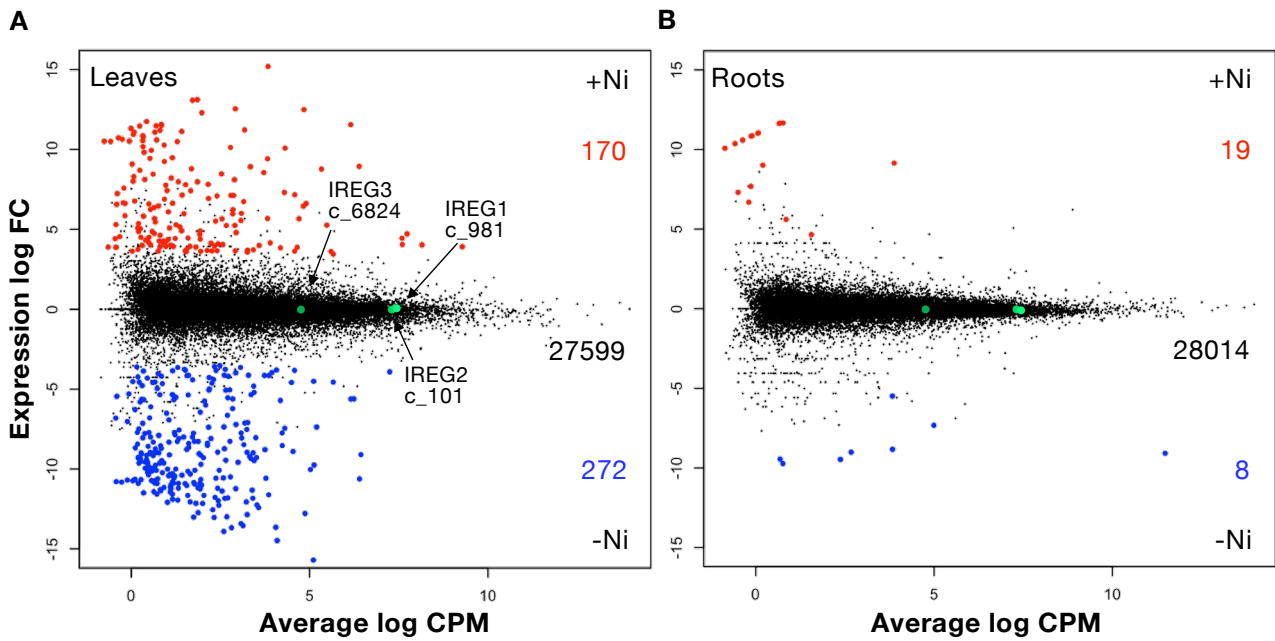


Fig. 1. Differential gene expression analysis in *Leucocroton havanensis* in response to nickel. MA plot showing comparative analysis in shoots (A) and roots (B) in the presence (+Ni) or absence (-Ni) of nickel using the Lhav_v2 transcriptome as reference. DE contigs up-regulated in response to nickel or the absence of nickel are colored in red and blue, respectively. Non DE contigs are colored in black. The number of contigs in each category is given on the right side of the panel. The positions of *LhavIREG1* (c_981), *LhavIREG2* (c_101) and *LhavIREG3* (c_6824) are marked with green dots. FC: fold change; CPM: counts per million.

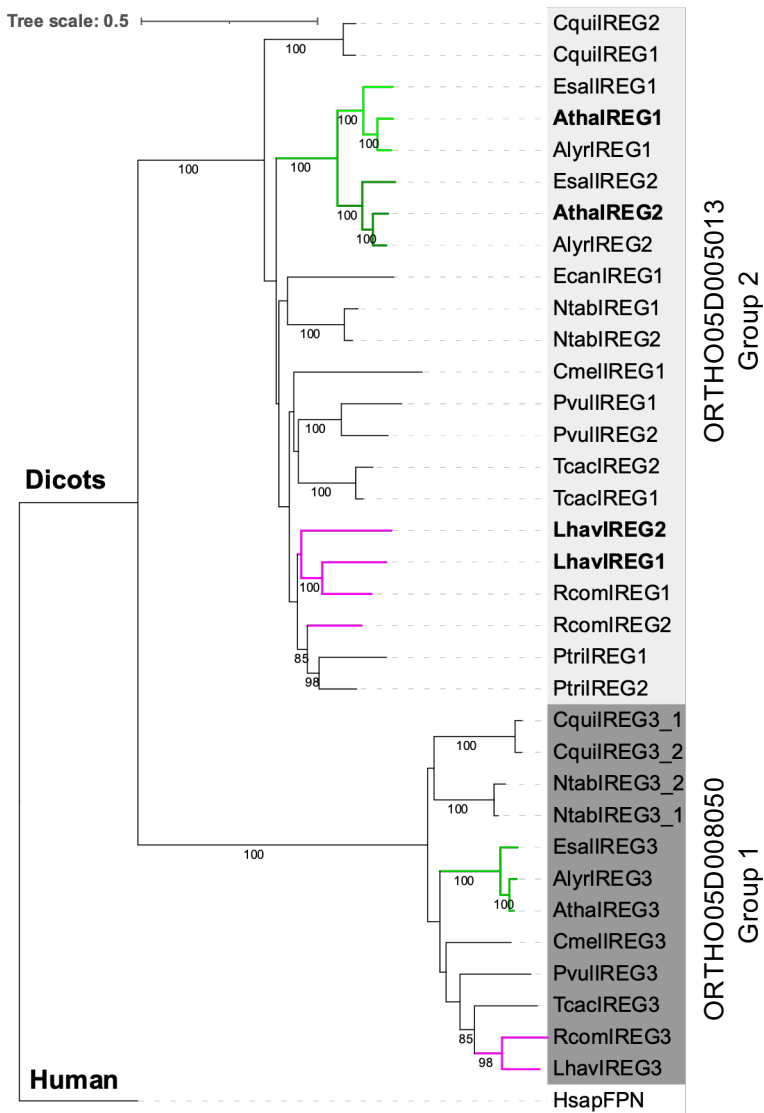


Fig.2. Phylogenetic tree of the IREG/FPN metal transporter family from Eudicots.

This tree includes IREG/FPN proteins from *Arabidopsis thaliana* (Atha, Brassicaceae), *A. lyrata* (Alyr, Brassicaceae), *Eutrema salsugineum* (Esal, Brassicaceae), *Teobroma cacao* (Tcac, Malvaceae), *Cucumis melo* (Cmel, Cucurbitaceae), *Phaseolus vulgaris* (Pvul, Fabaceae), *Nicotiana tabacum* (Ntab, Solanaceae), *Chenopodium quinoa* (Cqui, Amaranthaceae), *Erigeron canadensis* (Ecan, Asteraceae), *Ricinus communis* (Rcom, Euphorbiaceae), *Leucocroton havanensis* (Lhav, Euphorbiaceae). *Homo sapiens* (Hsap) ferroportin was used as an outgroup. Orthogroups ORTHO05D005013 and ORTHO05D008050 from Plaza 5 are shaded in light and dark gray, respectively. Clades containing Brassicaceae (green) and Euphorbiaceae (magenta) species are highlighted.

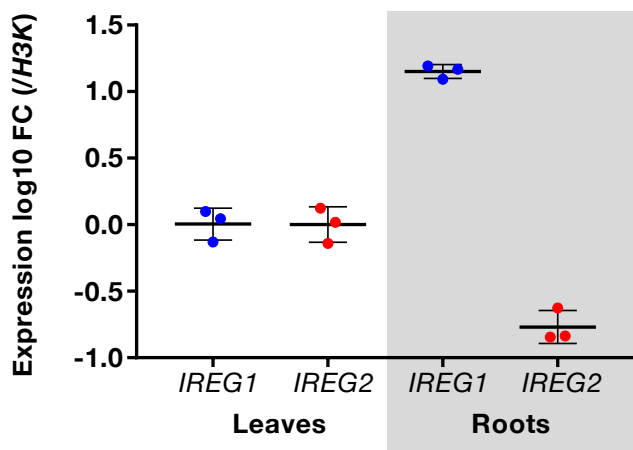


Fig. 3. Analysis of the expression of *LhavIREG1* and *LhavIREG2* in leaves and roots. Gene expression measured by RT-qPCR is expressed as log₁₀ fold change (FC) compared to *H3K* expression. Data are mean value \pm SD (n=3 independent samples).

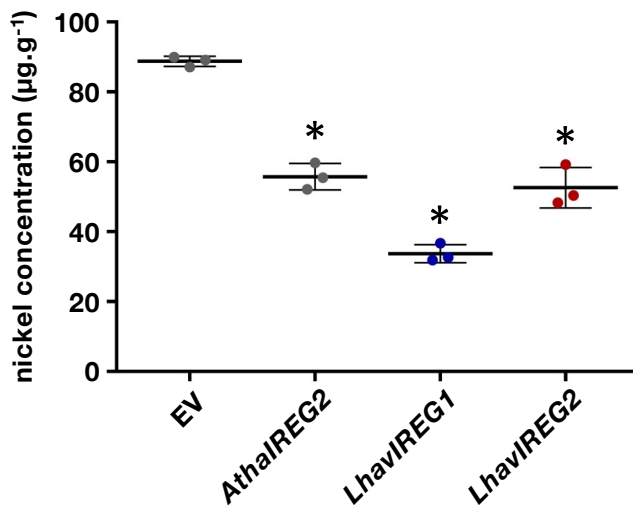


Fig. 4: Nickel accumulation in yeast cells expressing *LhaviREG1* and *LhaviREG2*. Nickel concentration was measured by MP-AES in yeast cells expressing *LhaviREG1*, *LhaviREG2* and *AthaIREG2* or transformed with pDR195 (EV). For each construct, the results are mean value \pm SD (n = 3; independent transformants). * $p < 0.01$ (Welch's t-test), compared with EV condition

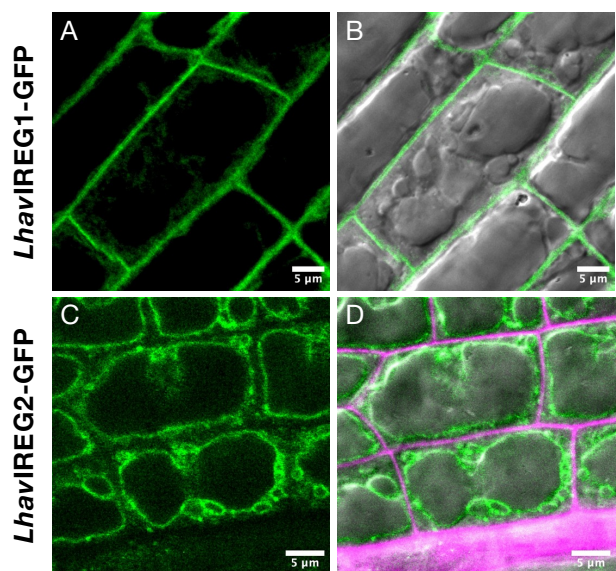


Fig. 5. Localization of *LhavIREG1* and *LhavIREG2* in plant cells. Root cells of *A. thaliana ireg2* mutant stably expressing *LhavIREG1*-GFP (A, B) and *LhavIREG2*-GFP (C, D) were imaged by confocal microscopy. GFP-associated fluorescence is shown in green (A, C). Corresponding composite images with DIC images are also shown (B, D). Propidium iodide Cell walls labelled with are shown in magenta. Scale bars are 5 μm.

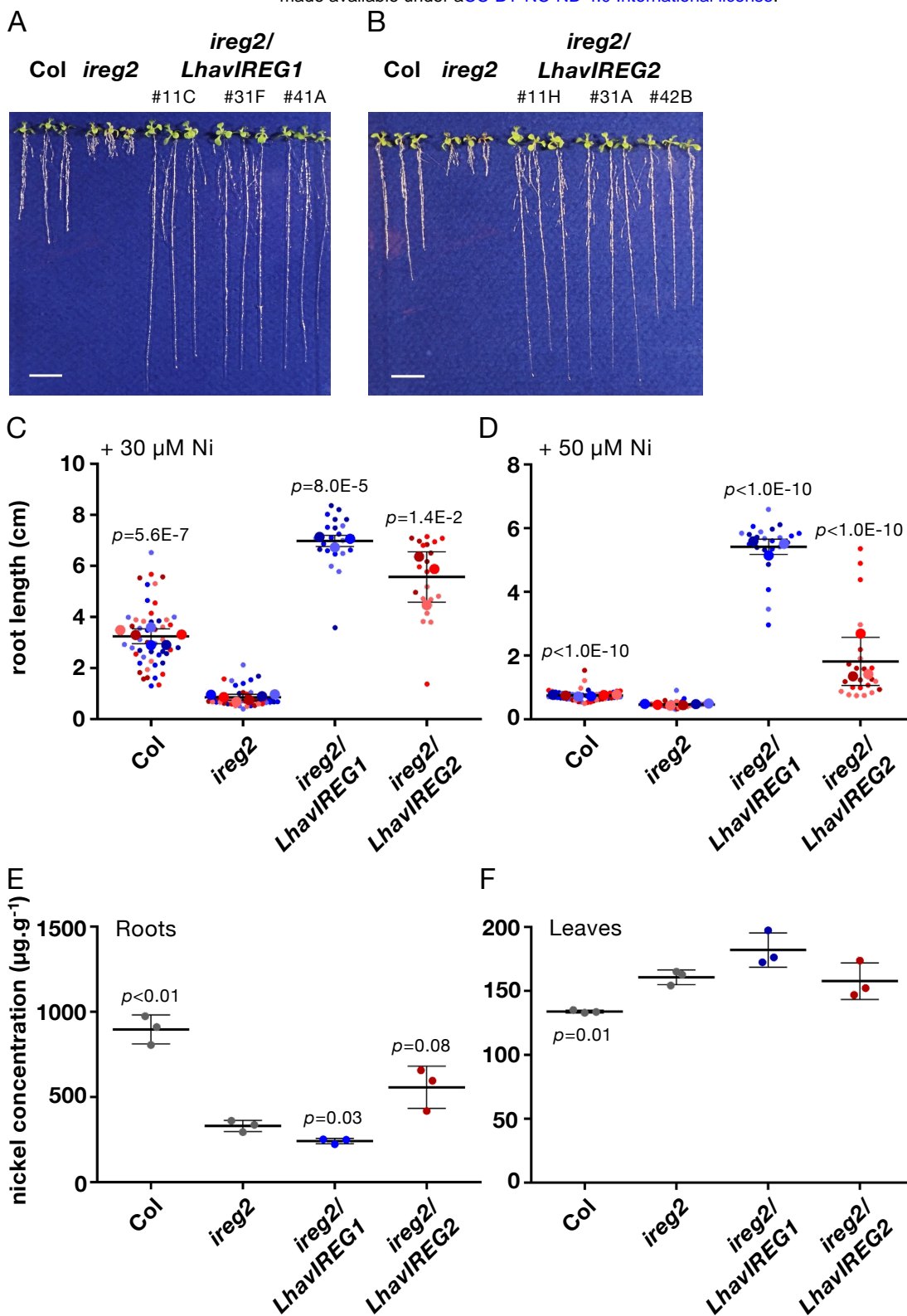


Fig. 6. Effect of LhavIREG1 and LhavIREG2 expression on nickel tolerance and accumulation. Pictures of individual *A. thaliana ireg2* transgenic lines expressing *LhavIREG1-GFP* (A) and *LhavIREG2-GFP* (B) grown on a culture medium containing 30 μM NiCl_2 for 10 days together with wild type (Col) and the *ireg2* mutant. Three representative plantlets were selected per line. Scale bars correspond to 1 cm. (C) Quantification of root growth of plantlets grown in the presence of 30 μM NiCl_2 and (D) 50 μM NiCl_2 . Each small dot represents an individual measurement. Large dots represent the mean value for each individual line or experiment. Means ($n=3$ independent transgenic lines, $n=6$ for Col and *ireg2*) \pm SEM are shown. p -values were calculated compared to *ireg2*. Nickel concentrations were measured in roots (E) and leaves (F) of the same genotypes. Data are mean value \pm SD ($n=3$ independent transgenic lines or experiments). p -values were calculated relative to *ireg2*.